Settlement-based cost optimization of geogrid-reinforced pile-supported foundation

C. Chen[1], F. Mao[2], G. Zhang[3], J. Huang[4], J.G. Zornberg[5], X. Liang[6] and J. Chen[7]

[1] *Professor, Hunan University, Key Laboratory of Building Safety and Energy Efficiency of the Ministry of Education, Changsha, PRC; Hunan University, College of Civil Engineering, Changsha, Hunan, PRC, E-mail: cfchen@hnu.edu.cn*
[2] *PhD Candidate, Hunan University, Key Laboratory of Building Safety and Energy Efficiency of the Ministry of Education, Changsha, PRC; Hunan University, College of Civil Engineering, Changsha, Hunan, PRC, E-mail: mfengshan@hnu.edu.cn*
[3] *Assistant Professor, Hunan City University, College of Civil Engineering, Yiyang, Hunan, PRC, E-mail: gbzhang@hnu.edu.cn (corresponding author)*
[4] *Associate Professor, The University of Texas at San Antonio, Department of Civil and Environmental Engineering, San Antonio, TX, USA, E-mail: jie.huang@utsa.edu*
[5] *Professor, The University of Texas at Austin, Department of Civil, Architectural, and Environmental Engineering, Austin, TX, USA, E-mail: zornberg@mail.utexas.edu*
[6] *Assistant Professor of Research, University at Buffalo, the State University of New York, Department of Civil, Structural and Environmental Engineering, Buffalo, NY, USA, E-mail: liangx@buffalo.edu*
[7] *Assistant Professor, Hunan University of Science and Technology, School of Information and Electrical Engineering, Xiangtan, Hunan, PRC, E-mail: chenjuan@hnust.edu.cn*

Received 14 August 2020, revised 26 November 2020, accepted 13 January 2021, published 13 July 2021

ABSTRACT: Cost optimization of Geogrid-Reinforced Pile-Supported Foundation (GRPSF) requires the minimum construction cost among all design alternatives within both ultimate limit state (ULS) and serviceability limit state (SLS) criteria. Usually, the optimization is conducted by selecting a limited number of design alternatives based on experience and then comparing them, which often does not lead to the real optimal design. This paper presents a novel optimization framework to systematically determine the design parameters to achieve the minimum construction cost for GRPSF, considering both ULS and SLS constraints that are relevant to post-construction performance and constructability. This framework is a hybrid of surrogate modeling and Finite Element Method (FEM) to calculate the post-construction settlement of GRPSF and search for the optimal design. Genetic Algorithm improved Black Hole Algorithm (BH-GA) was developed to determine the optimal values of design variables, including pile length and spacing, pile cap geometry, and geogrid layers and layout. The proposed approach can quickly identify the optimal design by exhausting all possible combinations of design parameters. Two well-documented case histories of GRPSF were redesigned using this framework, which validated its applicability and effectiveness in optimizing the design of GRPSF.

KEYWORDS: Geosynthetics, surrogate modeling, post-construction settlement, cost optimization, Geogrid-Reinforced Pile-Supported Foundation

REFERENCE: Chen, C., Mao, F., Zhang, G., Huang, J., Zornberg, J.G., Liang, X. and Chen, J. (2021). Settlement-based cost optimization of geogrid-reinforced pile-supported foundation. *Geosynthetics International*, **28**, No. 5, 541–557. [https://doi.org/10.1680/jgein.21.00002]

1. INTRODUCTION

Cost optimization of civil and infrastructure projects is a big concern for contractors and designers (Chikahiro *et al*. 2019; Jelušič and Žlender 2019, 2020; Song *et al*. 2020). Typically, the practice of optimization in geotechnical engineering involves forming a candidate pool of design alternatives and then comparing their costs. However, it is very difficult to develop a sufficient number of design alternatives that meet all safety and performance criteria (Aldwaik and Adeli 2014, 2017). The determination of many design parameters requires solving empirical or semi-empirical formulas in complicated, implicit formats, which are usually carried out by a trial-error approach. However, the situation becomes much more complicated when many components of a geotechnical structure interact with each other and the selection of one design parameter for one component has a global impact on the

selection of design parameters for other components. Therefore, it is not practical to conduct a chain of trial-error calculations inherent in an empirical/semi-empirical design framework and at the same time consider the design constraints of each design parameter.

The above-discussed issue is well encountered in the design of Geogrid-Reinforced Pile-Supported Foundation (GRPSF). GRPSF has been widely used to improve the bearing capacity and reduce settlements of weak subgrade that supports roadways, railways, and buildings. The types of piles commonly used in GRPSF include cement fly-ash gravel (CFG) columns (Zheng *et al*. 2008), driven piles (Huang *et al*. 2005; Girout *et al*. 2018; Wu *et al*. 2019; Shen *et al*. 2020), soil-cemented columns (Liu and Rowe 2015; Jamsawang *et al*. 2016), and stone columns (Ng and Tan 2015; Zheng *et al*. 2020). Currently, GRPSF is designed based on a semi-empirical method to estimate the bearing capacity and settlements (BSI 2010), which in general provides conservative and uneconomical results. Typically, the design is carried out in trial-error iterations to select a set of parameters, such as pile diameter and spacing, and geogrid arrangement, which are initially assigned and then varied until both bearing capacity and settlement criteria are met. The major disadvantage of this approach is that it relies heavily on the designer's experience and cannot exhaust all possible combinations. For instance, to increase the bearing capacity, either pile diameter or pile length can be increased, which may incur different increases in costs. There lacks a systematic approach to optimize the design.

Cost optimization of GRPSF aims at minimizing the cost, and at the same time, satisfying design constraints including, but not limited to, the post-construction settlement and the bearing capacity of pile and ground (Gary and Lucas 1987). However, three main hurdles challenge the cost optimization of GRPSF design. Firstly, it is difficult and, sometimes, impossible to determine the spatial variability of soil properties, soil-structure interface behavior, and load variations. This is the reason that empirical or semi-empirical methods are used to design GRPSF in most cases. Secondly, even though the design parameters are formulated in continuous mathematical equations, many of these parameters cannot be treated as continuous variables. For example, the number of geogrid layers, k, is only meaningful with non-negative integers, and pile length can only be varied at an increment of 0.1 m each time due to the constructability issue. A similar constructability constraint also applies to pile cap size, pile spacing, and pile diameter. Therefore, the optimization of GRPSF design is essentially a discrete-variable problem (Jelušič and Žlender 2018), which makes the commonly used gradient-based optimization methods unsuitable. Thirdly, boundary conditions are complex and difficult to determine in explicit equations, such as allowable post-construction and differential settlements (Wang *et al*. 2011; Chen and Zhang 2013). Model test has proved to be a powerful approach to optimize the arrangement of reinforcement, but its application is limited to the project that the cost of model test can be offset by the cost saving due to design optimization. (Ali *et al*. 2014; Li *et al*. 2019). The Finite Element Method (FEM) is often used as an alternative for determining the settlement of GRPSF during the construction and service stages (Han *et al*. 2007; Huang and Han 2010; Wijerathna and Liyanapathirana 2019), but it is too time-consuming to be used as a routine tool as it must scrutinize all possible combinations. Therefore, it is necessary to develop a more effective technique to search for the optimization design of GRPSF.

So far, the design optimization on geotechnical problems has not been well investigated. Some researchers extended the optimization method of structure designs to geotechnical designs including pile foundations (Leung *et al*. 2010; Ghalesari *et al*. 2015) and spread footings (Wang 2009), which adopted gradient-based methods that can be implemented by intelligent optimization algorithms. For piled composite foundations, the objective function was often defined by the total settlement or differential settlement (Liang *et al*. 2006; Bouassida and Carter 2014; Suro *et al*. 2016) and/or the construction cost (Gary and Lucas 1987; Jelušič and Žlender 2018; Narsavage 2019). It is noteworthy that the above-mentioned gradient-based approach can be implemented if the cost function and constraints are in explicit formulations.

For GRPSF, it has been found that the post-construction settlement often governs design, especially when the GRPSF is constructed on soft soil ground (Liu and Rowe 2015; Zhou *et al*. 2016). However, because the settlement of GRPSF is calculated using semi-empirical methods, it is hard to fit the settlement into an optimization model that requires a completely defined, continuous mathematic equation. Hence, a surrogate model (also named 'meta-model') (Slem and Tomaso 2018) was used as an effective alternative to determine the settlement in reliability analysis and optimization (Schoefs *et al*. 2013; Miro *et al*. 2014; Müthing *et al*. 2018; Zhao *et al*. 2019; Phutthananon *et al*. 2020). Various surrogate models (e.g. Polynomial Response Surface (PRS), Radial Basis Function (RBF), Kriging, Artificial Neural Network (ANN), and Support Vector Regression (SVR)) were reported to be able to tackle these problems in an effective and efficient manner (Bagheri *et al*. 2017; Goh *et al*. 2017; Zhang *et al*. 2017, 2019). The aforementioned successful applications justified the use of surrogate modeling to optimize the design of GRPSF as presented in this work.

To optimize GRPSF design, this paper presents a hybrid framework of Finite Element Method (FEM) and surrogate modeling. Essentially, it is a sort of machine learning approach to significantly reduce the demand for computational effort. FEM was used to generate a sample pool with limited data, while the surrogate model, which was implemented using an improved Black Hole-Genetic Algorithm (BH-GA) in this study, was used to derive the outcome of different design configurations and then optimize the design of GRPSF by selecting the optimal parameters. For optimization purposes, the construction cost was defined as objective function and GRPSF design parameters (e.g. pile length l_p, pile cap size a, pile spacing s, pile diameter d, pile cap thickness h, and the number of geogrid layers k) were variables in the optimization

process. The design constraints used in this paper were determined based on *Technical code for composite foundation of China* (MHURC 2012). After laying out the framework including the mathematical formulation and computational implementation procedure of the Kriging surrogate model and Black Hole-Genetic Algorithm, two case histories with field monitoring data were selected to validate the proposed framework.

2. MATHEMATICAL MODEL

2.1. Components of GRPSF

GRPSF is usually constituted of vertically installed piles (or columns), and horizontally installed cushion and/or geosynthetics, which are used to improve ground bearing capacity and minimize the differential ground settlement. Piles are used to transfer surcharge to competent soils (surrounding and/or underlying soils). Cushion and/or geosynthetics are used to facilitate distribution of surcharge between piles and soils with membrane effect and soil arching effect. The construction cost of GRPSF is substantially comprised of the material cost of piles and geosynthetics as well as the corresponding installation cost.

2.2. Design variables

Identification of all design variables is the first step to establish the optimization model of GRPSF. In the design practice of GRPSF, the height and width of an embankment are usually pre-determined in the planning phase based on traffic analysis. In addition, the size of the cushion may also be a fixed parameter, prior to the design of GRPSF, according to the classification of the roadway. Therefore, the sizes of the embankment and the cushion were not deemed as variables in this paper. The to-be-determined parameters encompass pile length l_p, pile cap size a (diameter for circular cap; edge length for square cap), pile spacing s (square arrangement in planar layout), pile diameter d, pile cap thickness h, and the number of geogrid layers k.

2.3. Cost function

The total construction cost of GRPSF, including installation and material costs, was defined in the objective function, as expressed in Equation (1):

$$\text{Minimize cost } Q(\boldsymbol{x}) = f\left(l_p, a, s, d, h, k\right) \tag{1}$$

It should be noted that the construction cost in Equation (1) depends on the local price of materials and the selection of construction methods. The design optimization of GRPSF is essentially a search for the variable vector $\boldsymbol{x} = (l_p, a, s, d, h, k)$ that leads to the minimum construction cost shown in Equation (1) and, at the same time, meets constraints.

2.4. Constraints

The constraints of this optimization problem can be categorized into three classes: site conditions, design specifications, and construction requirements. Taking the Pre-stressed High-Strength Concrete (PHC) pile as an example, its maximum length depends on the depth of the bearing stratum, and its diameter can only be of 0.3, 0.4, or 0.5 m due to constructability issues. Additionally, the selection of design states, – that is, ultimate limit state (ULS) (e.g. bearing capacity of foundation and reinforcement) or serviceability limit state (SLS) (e.g. settlement, differential settlement), would also lead to different constraints in optimization. The constraints used in this work are described in detail hereafter.

According to design and construction practice, the reasonable range ($\boldsymbol{x}_{\text{lower}}$, $\boldsymbol{x}_{\text{upper}}$) for each design variable was first determined. Because PHC piles would be used as vertical supports of GRPSF in the cases presented in this work, the design variables related to such piles will be discussed and analyzed in this paper. Specifically, the pile length varies at a minimum increment of 0.1 m, and its diameter can be of 0.3, 0.4, or 0.5 m (MHURC 2012). In addition, PHC piles are usually equipped with square caps; the recommended area replacement ratio of piled embankments ranges from 0.15 to 0.25; the recommended thickness of pile cap ranges from 0.3 to 0.5 m; and the minimum net span between neighboring pile caps is 0.5 m. The layout of piles is required to render a ratio of pile spacing to pile diameter in a range from 5 to 8. Geogrid could be used up to 3 layers.

Besides the aforementioned linear constraints, the optimization of GRPSF is further subjected to a number of non-linear constraints, as presented in design codes (MHURC 2012), which include bearing capacity of the subgrade, axial load capacity of piles, shear and moment capacity of pile caps, and post-construction settlement.

The requirement on the bearing capacity is expressed as:

$$p_z + p_{cz} \leq f_{az} \tag{2}$$

where p_{cz} is the soil overburden stress; p_z is the additional stress induced by loading; f_{az} is the allowable bearing capacity.

Although Equation (2) was used to ensure soil stability at the base of the embankment and at the tip of the pile, they were treated differently in the calculation. At the tip of the pile, the pile group and the soil between piles are assumed to be a coherent block, acting as an equivalent footing, and the bearing capacity is solely dependent on the soil underlying the pile tip. In contrast, at the base of the embankment the piles and the surrounding soil form a composite foundation and its bearing capacity is defined as a function of pile axial load capacity and soil bearing capacity, which is indicated in Equation (3):

$$f_{az} = \beta_p m \frac{R_a}{A_p} + \beta_s (1 - m) f_{sk} \tag{3}$$

where R_a is the ultimate bearing capacity of the single pile; f_{sk} is the capacity of surrounding soil; A_p is the cross-section area of a pile; m is the area replacement ratio; and β_p and β_s are the corrective factors for pile and surrounding soil, respectively.

The requirement on bearing capacity of the individual pile is presented in Equation (4)

$$R_s \leq R_a \tag{4}$$

where R_s is the axial load applied on the single pile. It is noteworthy that the negative skin friction could contribute to the vertical load if there is any.

The pile cap transfers the embankment loads to the pile by resisting bending moment and shearing force (including cross-sectional shear and punching shear), which shall not exceed the limits:

$$M \leq M_R \tag{5}$$

$$V \leq V_R \tag{6}$$

where M_R and V_R are the moment and shear resistance of pile cap, respectively; M and V are the moment and shear force on pile cap, respectively.

As required by service limit state (SLS), the post-construction settlement of GRPSF, $s_{\text{post-construction}}$, should not exceed the allowable value $[\Delta s]$, as expressed by

$$s_{\text{post-construction}} \leq [\Delta s] \tag{7}$$

Among the above non-linear constraints, the constraints related to the bearing capacity (i.e. GRPSF, individual pile, and pile cap) can be calculated explicitly, while the post-construction settlement is difficult to calculate directly. Conventionally, the layer summation method can be used to calculate the settlement when the pile spacing is small, while in contrast the Mindlin method (Geddes 1966) is suitable when the pile spacing is large. However, both methods were primarily developed for building foundations so they cannot consider some factors of GRPSF, such as layers of geosynthetic reinforcement. The Finite Element Method (FEM) provides a powerful tool to calculate the settlement of GRPSF; however, exhausting all variable combinations to search for the optimum is formidable in terms of computational time. As an alternative, surrogate modeling with the assistance of data from FEM was established using a regression relationship between the settlement and design variables to solve the post-construction settlement of GRPSF, which can significantly reduce the demand for computational capacity.

3. SURROGATE MODELING OF POST-CONSTRUCTION SETTLEMENT

Among the family of surrogate models, the Kriging model was a stochastic approach, originally developed to determine mineral distribution and estimate reserves (Krige 1953), which has recently been extensively applied to optimization problems and reliability analysis in multidisciplines such as aerospace, automobile, and civil engineering (Hawchar *et al.* 2018). According to the Kriging model, the response $y(\boldsymbol{x})$ at a point can be linearly interpolated from the linear summation of the weighted response of sampling points, which is written as:

$$\hat{y}(\boldsymbol{x}) = \sum_{i=1}^{n} \lambda_i y_i \tag{8}$$

where λ_i is the ith weight coefficient, and y_i is the response of the ith sampling point.

Aiming at calculating the weight coefficient λ, the unknown function $Y(\boldsymbol{x})$ was assumed a stochastic process (Sacks *et al.* 1989):

$$Y(\boldsymbol{x}) = F(\boldsymbol{x}, \beta) + \mathrm{Z}(\boldsymbol{x}) = f^T(\boldsymbol{x})\beta + \mathrm{Z}(\boldsymbol{x}) \tag{9}$$

where $F(\boldsymbol{x}, \beta)$ defines the deterministic part of the regression model that characterizes an approximate global trend over the whole design domain with a regression coefficient β; $\mathrm{Z}(\boldsymbol{x})$ denotes the stochastic process with a mean value of zero and a variance of σ^2.

The spatial correlation function of a variable is given by

$$R(\boldsymbol{x}_i, \boldsymbol{x}_i') = \prod_{i=1}^{m} \exp(-\theta_i |\boldsymbol{x}_i - \boldsymbol{x}_i'|^2) \tag{10}$$

where $R(\boldsymbol{x}_i, \boldsymbol{x}_i')$ is the Gaussian correlation function between two samples; θ is the undetermined parameter that characterizes the spatial correlation between samples, of which the length is equal to the dimension of the variable $\boldsymbol{x}$.

Using DACE toolbox in MATLAB (Lophaven *et al.* 2002), the parameters of the Kriging surrogate model as defined in Equation (8) can be calculated. Different from other surrogate models, both the predicted value and variance are outputs when the Kriging model is used to predict responses at arbitrary sites. The variance indicating the deviation of predicted values will be used in the following sections.

Using the Kriging surrogate model established above, the post-construction settlement of GRPSF design solutions can be determined much more efficiently than the FEM computations. The enormous computational consumption in FEM modelings was remarkably reduced for solving post-construction settlement corresponding to the large amount of design alternatives (i.e. combinations of design variables). Because the post-construction settlement is limited in design of GRPSF as a critical constraint, the cost optimization can be implemented efficiently with all design constraints met in a straightforward way.

4. BH-GA OPTIMIZATION ALGORITHM

4.1. Black Hole (BH) algorithm

BH algorithm is a novel, nature-inspired metaheuristic algorithm based on the black hole phenomenon and originating from population-based algorithm Particle Swarm Optimization (PSO) (Zhang *et al.* 2008). As featured in other population-based algorithms, the candidate solutions to the problem are generated randomly in a search space and the best candidate is defined as the black hole in each iteration. The candidates in BH algorithm can be regarded as the stars in the universe. All solutions would move towards the best candidate in the search space, which is analogous to the process of the black hole

absorbing the stars. The BH algorithm (Zhang *et al*. 2008) was originally proposed to introduce a new mechanism to accelerate the convergence velocity of particle swarm optimization (PSO), but was found insufficient without considering the event horizon of the black hole and destruction of stars.

Hatamlou (2013) improved the BH algorithm by defining the updated formula of the star's location and the radius of the event horizon R_{BH} respectively, as seen in Equations (11) and (12). The distance of the candidate closer than R_{BH} would be sucked into the black hole, and then a new candidate would be born to maintain the population size. All the stars $\boldsymbol{x}_i$ would move towards the black hole $\boldsymbol{x}_{BH}$ by applying Equations (11) and (12).

$$\boldsymbol{x}_i(t+1) = \boldsymbol{x}_i(t) + \text{rand}(0,1) \times (\boldsymbol{x}_{BH} - \boldsymbol{x}_i(t)); \quad i = 1, \ldots, N \tag{11}$$

$$R_{BH} = \frac{f_{BH}}{\sum_{i=1}^{N} f_i} \tag{12}$$

where $\boldsymbol{x}_i(t)$ and $\boldsymbol{x}_i(t+1)$ denote the positions of the ith star at the tth and $(t+1)$th iteration, respectively; $\boldsymbol{x}_{BH}$ denotes the position of the black hole in the search space; rand (0,1) defines a random number between 0 and 1; N corresponds to the number of stars; f_i and f_{BH} are the fitness values of ith star and the black hole, respectively.

4.2. BH-GA algorithm

As a simplification of PSO, the BH algorithm exhibits high computational efficiency for some simple cases but may not be effective for cases with multi-modal optimization or involving discrete variables (Piotrowski *et al*. 2014). To improve the BH algorithm, learning factors r_1 and r_2 that are between zero and one were introduced into the location update formula of stars under the absorption of the black hole. Accordingly, Equation (12) can be rewritten as:

$$\boldsymbol{x}_i(t+1) = r_1\boldsymbol{x}_i(t) + r_2\text{rand}(0,1) \times (\boldsymbol{x}_{BH} - \boldsymbol{x}_i(t)); \quad i = 1, \ldots, N \tag{13}$$

Additionally, Genetic Algorithm (GA) (Michalewicz and Janikow 1991) was incorporated with BH to achieve a novel BH-GA algorithm with an enhanced search capability on both local and global space. Specifically, the selection and crossover operations featured in GA were introduced into BH-GA to improve the convergence efficiency and accommodate problems with either continuous or discrete variables. The BH-GA algorithm was executed in the following steps:

(*a*) Initialize the values of r_1, r_2 and the position of population $\boldsymbol{x}_i$ within the allowable range $(\boldsymbol{x}_{lower}, \boldsymbol{x}_{upper})$.

(*b*) Locate the position of the best-fit individual $\boldsymbol{x}_{best,t}$, which will be identified as the black hole in the tth iteration; determine the radius of the event horizon R_{BH} of the black hole per Equation (12); update the positions of the whole population per Equation (13). If the distance between one individual and the black hole is less than R_{BH}, the individual will be absorbed by the black hole and a new particle will be generated in the variable space; if one individual is found with better fit than that of $\boldsymbol{x}_{best,t}$ on its route moving towards the black hole, it will be identified as the black hole in the $(t+1)$th iteration, – that is $\boldsymbol{x}_{best,t+1}$.

(*c*) Evaluate the fit of each individual in the tth iteration, and select and crossover candidates by the ranking of fit evaluation to generate the evolved individual in the $(t+1)$th iteration per Equation (14). Only the top 97% individuals are picked out to generate the next generation, and $N \times 3\%$ new samples are generated to maintain the size of population.

$$\boldsymbol{x}_1^{t+1} = r_3\boldsymbol{x}_1^t + (1 - r_3)\boldsymbol{x}_2^t$$

$$\boldsymbol{x}_2^{t+1} = r_3\boldsymbol{x}_2^t + (1 - r_3)\boldsymbol{x}_1^t \tag{14}$$

where r_3 is the crossover value defined by rand (0,1).

(*d*) Repeat steps b-c until at least one of the following convergence criteria is met: the terminative number of iterations is reached, or the black hole fails to update for the designated number of iterations.

4.3. Examination using benchmark functions

Benchmark functions (unimodal: F1, F2, F3 and F4; and multimodal: F5, F6, and F7) selected from Suganthan *et al*. (2005) were used to examine the optimization capability of the presented BH-GA algorithm. The function expressions, definition range, and other relevant information for these benchmark functions are presented in Table 11. Note that the dimension of the variable vector ($D = 10$) was used for all benchmark functions. If the benchmark function has continuous variables, the minimum variation of variables was set equal to the default computational precision (10^{-16}). If the benchmark test function possesses discrete variables, the minimum variation of variables was set to 0.1. Each benchmark function was solved using four optimization methods/algorithms including BH-GA, BH, GA and PSO to compare their performance and applicability. For all algorithms, the population number N was initialized to 200, and the terminated number of iterations was set to 300.

The computational results of the seven benchmark functions using four optimization algorithms are shown in Table 12. Specifically, BH-GA algorithm exhibited its effectiveness for both discrete-variable and continuous-variable optimizations. In contrast, GA manifested an excellent performance in continuous-variable optimization, in which the evolution of the population depended largely on the crossover operation. With the same underlying fundamentals, PSO performed less efficiently than BH for most functions, which could be attributed to the excessive emphasis on the global exploration capability in PSO.

To evaluate the performance of the algorithm, the evolution of fitness over the generation for the seven benchmark functions is shown in Figure 10. The fastest

convergence speed can be observed in the case using BH-GA, compared with other algorithms (BH, GA and PSO) for both continuous- and discrete-variable problems. It is noteworthy that all the presented algorithms perform less efficiently in optimizing discrete-variable problems than in optimizing continuous-variable problems. It is reasonably recognized that the discrete-variable search needs much more time than the continuous-variable search when solving the same benchmark function due to less local information included in a discrete-variable problem. The competitiveness of BH-GA in dealing with discrete-variable problems lies in the introduction of the crossover operation that improves exploitation and exploration efficiency substantially.

4.4. Examination using classical engineering problems

To further investigate the performance of the BH-GA, two reported optimization problems of engineering application were applied in order to examine the improved algorithm BH-GA. Details for the two optimization problems can be found in Figure 11 and Equations (16) and (17). The first problem is the cost optimization of a pressure vessel (Sandgren 1990), aiming at minimizing the fabrication cost including material, forming, and welding. Another structural optimization problem was to minimize the weight of a cantilever beam (Chickermane and Gea 1996). The design variables included the dimensions for the outer shape of five components (see Figure 11b).

The presented BH-GA algorithm as well as GA, BH and PSO were applied respectively to search the optimal design variables for the two structural optimization problems. The optimization results of the above four algorithms as well as the one using MVO (Multi-Verse Optimizer) reported in Seyedali *et al.* (2015) are presented in Tables 13 and 14. For the pressure vessel, it was found that design variables optimized by BH-GA lead to the minimum cost compared with the other four algorithms. Additionally, the minimum weight of the cantilever beam was also provided by BH-GA. Hence, in terms of effectiveness and efficiency, the applicability of the presented BH-GA algorithm to optimization problems in engineering applications with complex constraints was scrutinized.

5. PROCEDURE OF OPTIMIZATION DESIGN

Optimization of GRPSF design can be carried out by incorporating the aforementioned Kriging surrogate modeling and BH-GA search algorithm in the steps described below (see Figure 1).

Step 1: Determine the bounds ($\boldsymbol{x}_{\text{lower}}$, $\boldsymbol{x}_{\text{upper}}$) of design variables $\boldsymbol{x} = (l_p, a, s, d, h, k)$ in the specific engineering case, and define Equation (1). Specifically, based on Chinese codes and construction experience, the lower bounds of design variables shall be $\boldsymbol{x}_{\text{lower}} = (10, 0.8, 1.5, 0.3, 0.3, 0)$, and the upper bound $\boldsymbol{x}_{\text{upper}}$ could be designated and justified using semi-empirical methods as stated previously in Section 2.3.

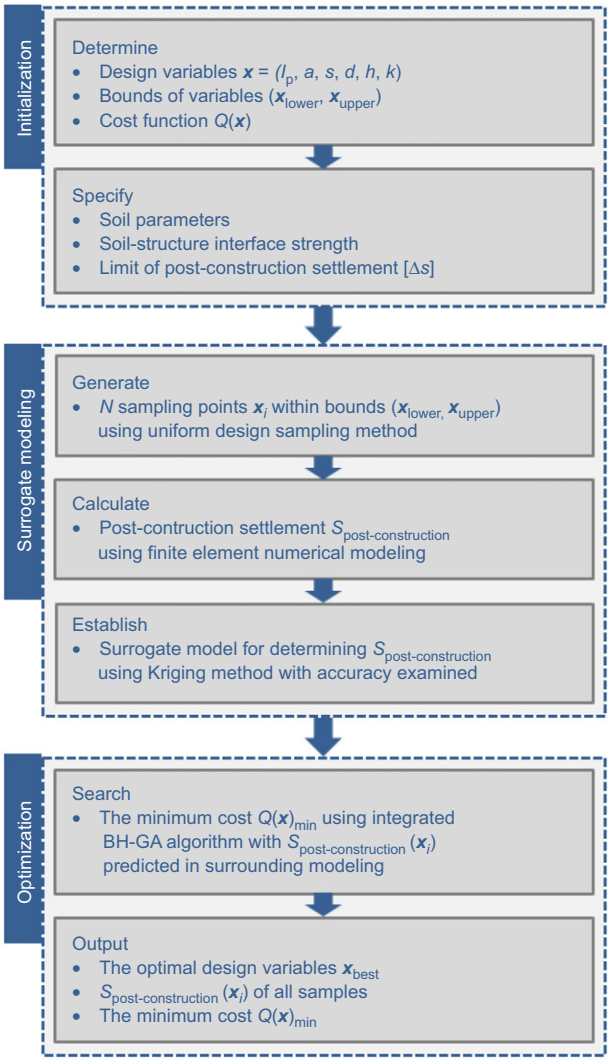

Figure 1. Flowchart for optimization design of GRPSF

Step 2: Set the values of parameters in constraints, – for example, the bearing capacity of native soils f_{sk}, the skin friction of pile embedded in various soil layers, the limit of post-construction settlement[Δs], and so on.

Step 3: Complete surrogate modeling aiming at calculating the GRPSF settlement: generate the sampling of design variables (i.e. training sample pool) using appropriate sampling methods (e.g. uniform design, orthogonal design, and the Latin hypercube method); determine the response (post-construction settlement) of each sample point using numerical modeling (i.e. FEM); establish the Kriging surrogate model based on the training samples; set the tolerance and examine the surrogate model using extra sample points (i.e. prediction samples), which is a process to validate the surrogate model by comparing the predicted response from the surrogate model with the calculated response from FEM; add the prediction samples into the training sample pool and repeat the above operations until the predicted–calculated difference is less than the tolerance.

Step 4: Search the minimum construction cost (Equation (1)) using the BH-GA algorithm with constraints treated by a penalty function method, in which the settlement of GRPSF can be determined using the

surrogate model in the preceding step. The cost Q of the sample located in the infeasible field is attributed with the value of 1×10^5 USD/m, which can be identified as impractical fitness for construction cost of GRPSF cases.

Step 5: Terminate the search if the iteration limit is reached or the search converges, and output the $\boldsymbol{x}_{best} = (l_p, a, s, d, h, k)$ and corresponding construction cost Q_{min}.

Two case histories have been selected to validate the proposed framework to optimize GRPSF design, which will be discussed thoroughly in this section.

6. CASE STUDY

6.1. Case history A: PHC pile-supported GRPSF

6.1.1. *Description*

The GRPSF of K13 + 320 section of the XING-SHAN highway project in Guangdong, China (TPDI 2016) was redesigned as an example to demonstrate the effectiveness of the presented design optimization framework. In this case, the native subgrade was profiled by a 14.4 m-thickness soft soil layer underlying a 3 m-thickness deposit soil layer. The water table was located 1.3 m below the ground surface. As shown in Figure 2, the embankment was 7 m in height and had a crest width of 26 m, which was bounded by two sides 1 : 1.5 slopes (vertical: horizontal). Without any improvement, the subgrade soil would settle 0.7 m after the completion of the 7 m embankment. Hence, GRPSF was selected to improve the subgrade to reduce excessive settlement. The original design and soil layer information are schematically illustrated in Figure 3. Site investigation, mainly consisting of borehole sampling and Standard Penetration Test (SPT), provided soil properties of each soil layer, which are listed in Table 1.

6.1.2. *Finite Element modeling parameters*

Constitutive models and their parameters used to simulate GRPSF were determined from either in situ and laboratory tests (TPDI 2016) or relevant literature (Wu *et al.* 2019), as shown in Table 2.

Modified Cam Clay (MCC) was used to model the soft clay and the relevant parameters were obtained from one-dimensional consolidation tests (κ, λ, and e_1) and

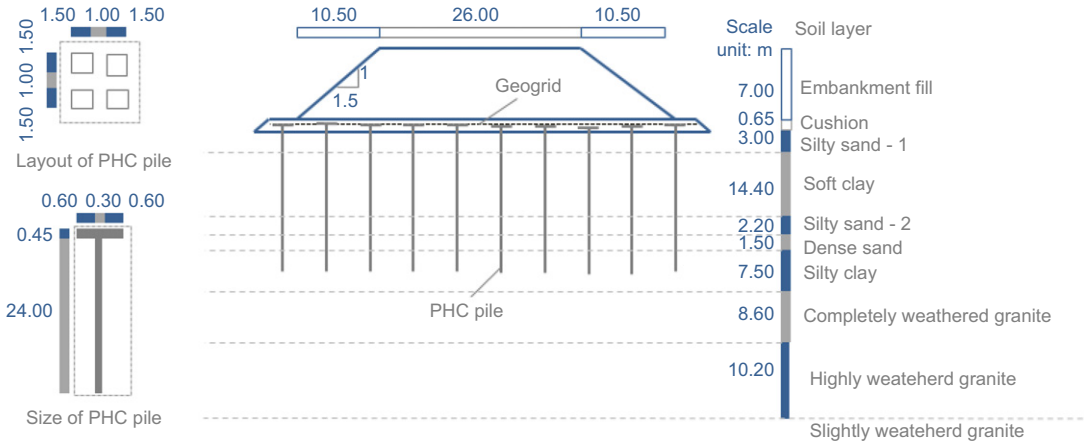

Figure 2. Cross-sectional schematic of GRPSF for case history A

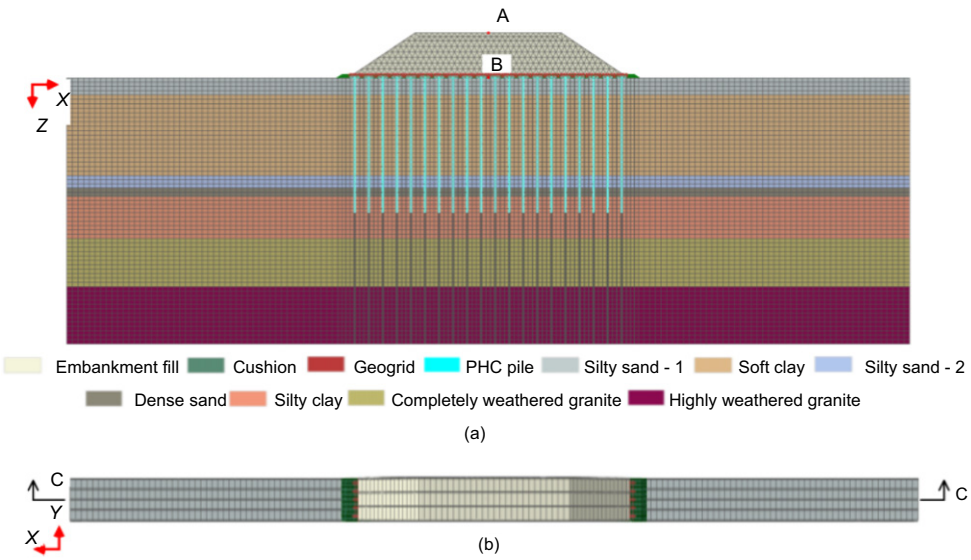

Figure 3. Schematic of mesh and grid of case history A: (a) section C-C; and (b) top view

Table 1. Physical and mechanical characteristics of soil layers

Soil layer	D (m)	LL (%)	PL (%)	PI (%)	LI (%)	w (%)	ρ (g/cm^3)	S_r (%)	e	c_c	N_{spt}
Silty sand-1	0–3	—	—	—	—	—	20	—	0.70	—	12
Soft clay	3–17.4	51.2	28.3	23.0	0.79	46.1	16	100	1.65	1.85	3
Silty sand-2	17.4–19.6	—	—	—	—	—	19	—	0.9	—	9
Dense sand-1	19.6–21.1	—	—	—	—	—	18	—	0.60	—	—
Silty clay	21.1–28.6	33.2	23.5	9.7	0.42	27.6	18	90	0.83	0.50	37
Highly weathered granite	28.6–37.2	33.8	21	12.8	0.29	24.7	19	92	0.73	0.37	40
Highly weathered granite	37.2–47.4	—	—	—	—	—	20	—	0.70	—	57
Embankment backfill	7	—	—	—	—	—	18	—	—	—	—

Notes: D: depth of soil layer; LL: liquid limit; PL: plastic limit; PI: plasticity index; LI: liquid index; w: moisture content; ρ: density; S_r: degree of saturation; e: void ratio; c_c: coefficient of compressibility; N_{spt}: SPT blow counts.

Table 2. Physical and mechanical parameters for FE modeling

Material	Model	E (MPa)	v	c (kPa)	ϕ (°)	λ	κ	M	e_1	k_p (cm/s)
Subsurface soils										
Silty sand-1	MC	11.1	0.33	6	34	—	—	—	—	2.8×10^{-3}
Soft clay	MCC	—	—	—	—	0.09	0.013	0.43	1.31	4.0×10^{-7}
Silty sand-2	MC	18.6	0.33	5	32	—	—	—	—	1.2×10^{-3}
Dense sand	MC	18.6	0.3	2	38	—	—	—	—	1.5×10^{-5}
Silty clay	MC	4.5	0.3	16	18	—	—	—	—	6.0×10^{-5}
Completely weathered granite	MC	20	0.3	25	25	—	—	—	—	2.0×10^{-3}
Highly weathered granite	MC	23	0.3	28	28	—	—	—	—	7.0×10^{-3}
Backfill material										
Embankment	MC	20	0.33	20	28	—	—	—	—	—
Cushion	MC	50	0.33	2	36	—	—	—	—	—
Basal reinforcements										
Geogrid	EP	$T_{rupture}$ = 80 kN/m at strain of 13%								
		Piling								
Pile	E	30 000	0.2	—	—	—	—	—	—	—

Notes: E: Young's modulus; v: Poisson's ratio; c: cohesion; ϕ: friction angle; λ: gradient of virgin consolidation line; κ: gradient of swelling line; M: stress ratio; e_1: intercept; k_p: permeability coefficient; $T_{rupture}$: rupture strength of geogrid.

Table 3. Bounds and increments for design variables

Design variable	l_p, (m)	a (m)	s (m)	d (m)	h (m)	k
Lower and upper bounds	(10, 26.1)	(1, 1.7)	(1.8, 2.9)	(0.3, 0.5)	(0.3, 0.5)	(1, 3)
Increment	0.7	0.1	0.1	0.1	0.1	1

Notes: l_p: pile length; a: pile cap size; s: pile spacing; d: pile diameter; h: pile cap thickness; k: the number of geogrid layers.

consolidated undrained (CU) triaxial compression tests (stress ratio M). The remaining soil layers, embankment backfill, and sand cushion were modeled as a Mohr-Coulomb (MC) model with zero dilation angle. The PHC pile was idealized as homogeneous and linear elastic material, and the geogrid was assumed as linear elastic-perfect plastic (EP) material with a rupture strength of 80 kN/m at a strain of 13%.

6.1.3. *Uniform design of sampling space*

According to soil profile and properties in Table 2 as well as constraints previously given, the design variables with their variation range and increments used in the discrete-variable search for the case are listed in Table 3. The determination of the variable range will be discussed in detail hereafter.

(*a*) Pile length, l_p: Design practice experience suggests that using PHC pile with a length greater than 10 m in GRPSF tends to result in the most economical solution compared with other alternatives, such as soil-cemented pile or auger cast concrete pile. Meanwhile, soil profile indicates that PHC pile with length greater than 25.5 m will render the pile tip in a competent sand-gravel layer (dense sand-2), which will lead to negligible settlement of GRPSF. Thus, l_p is limited between 10 and 26.5 m.

(*b*) Pile diameter, d: The commonly used diameters for PHC pile in practice are 0.3, 0.4, or 0.5 m, as

suggested in the design codes of PHC piles (MHURC 2012).

(*c*) Pile spacing, *s*: The distance between neighboring piles is recommended to be 5–8 times the pile diameter in Chinese code *Technical code for composite foundation* (MHURC 2012), which is used as the lower and the upper bounds of pile spacing, respectively.

(*d*) The number of geogrid layers, *k*: The use of geogrid is highly recommended as horizontal reinforcement and is limited to three layers for GRPSF (MHURC 2012).

(*e*) The thickness of pile cap, *h*: Shear and moment bearing capacity requirements of the pile cap, defined in Equations (4) and (5), govern the thickness; according to the recommendations regarding the application of PHC piles to GRPSF in design codes (MHURC 2012), the thickness of pile cap could be 0.3, 0.4, or 0.5 m.

(*f*) Pile cap size, *a*: The replacement ratio, defined as the ratio of the area of a pile cap to its tributary area, varies between 0.15 and 0.45.

Samples were evenly selected from the design space to achieve as uniform a distribution as possible, considering the boundary and increment of each variable. (Note: one design configuration constitutes one sample). In total, twenty-five samples were generated, which are listed in Table 4. Note that the last sample (i.e. Sample 25) is the real case that contains all as-built parameters and will be used to assess the effectiveness of the surrogate model.

Table 4. Samples generated using uniform design sampling including original design solution

Sample	l_p (m)	*a* (m)	*s* (m)	*d* (m)	*h* (m)	*k*
1#	10.0	1.0	2.1	0.4	0.4	3
2#	10.8	1.1	2.4	0.5	0.5	2
3#	11.6	1.2	2.8	0.3	0.4	1
4#	12.4	1.3	1.9	0.5	0.5	1
5#	13.2	1.4	2.2	0.3	0.4	3
6#	14.0	1.5	2.6	0.4	0.5	2
7#	14.8	1.6	2.9	0.3	0.4	1
8#	15.6	1.7	2.0	0.4	0.5	1
9#	16.4	1.0	2.4	0.5	0.3	3
10#	17.2	1.1	2.7	0.4	0.5	2
11#	18.0	1.2	1.8	0.5	0.3	2
12#	18.8	1.3	2.2	0.3	0.5	1
13#	19.6	1.4	2.5	0.5	0.3	3
14#	20.4	1.5	2.9	0.3	0.5	2
15#	21.2	1.6	2.0	0.4	0.3	2
16#	22.0	1.7	2.3	0.3	0.5	1
17#	22.8	1.0	2.7	0.4	0.3	3
18#	23.6	1.1	1.8	0.5	0.4	3
19#	24.4	1.2	2.1	0.4	0.3	2
20#	25.2	1.3	2.5	0.5	0.4	1
21#	26.0	1.4	2.8	0.3	0.3	3
22#	26.8	1.5	1.9	0.5	0.4	3
23#	27.6	1.6	2.3	0.3	0.3	2
24#	28.4	1.7	2.6	0.4	0.4	1
25#	24.0	1.5	2.5	0.3	0.3	2

6.1.4. *Response of numerical modeling*

Numerical modeling of the case was carried out in ABAQUS using the parameters of each sampling indicated in Table 4. The schematic of this numerical model is illustrated in Figure 3. To save computational time, the dimension in the longitudinal direction of the embankment (*Y* direction in the model) was equal to one pile spacing. The transverse dimension (*X* direction in the model) was set to be three times the embankment width to eliminate the boundary effect, as shown in Figure 3.

The model was extended to the top of a slightly weathered granite layer. According to the in situ investigation, the slightly weathered granite layer had an rock quality designation greater than 90%; therefore, the model assumed a fixed, impermeable bottom boundary.

PHC piles with hollow sections were converted into equivalent solid sections based on the principle of equal compressive stiffness EA, where E is the elastic modulus and A is the cross-sectional area. Embankment backfill, PHC pile, and foundation soils were modeled using C3D8 elements, while the geogrid embedded in the sand cushion was modeled using truss element T3D2. Additionally, no slip between the geogrid and the sand cushion was allowed. The pile–soil interaction was modeled by Coulomb's frictional interface element: relative displacement was not allowed if shear stress was less than shear strength and would be allowed if shear stress exceeded the shear strength that was proportional to the normal pressure.

Since it is a highly non-linear problem involving large deformations, the unsymmetrical matrix quasi-Newton technique was employed to accelerate the convergence. The staged construction process of the embankment was simulated by constructing embankment by lifts. The modeling consisted of the following steps: (a) the geostatic stress of the strata was initiated; (b) the incurred displacement was zeroed out once the in situ field was established; (c) geogrid, sand cushion, and PHC piles were installed; (d) the embankment was constructed in lifts; and (e) consolidation was allowed for the first half-year under embankment load and then the following thirty years under an additional surcharge of 15 kPa. The simulation terminated at 30 years in service since the degree of consolidation was nearly 100% and the settlement at the base of the embankment became less than 0.1 mm/year. Over a hundred thousand nodes were included in the mesh, and it took around five hours to complete the three-dimensional analysis for each model using parallel acceleration with an 8-core processor (Intel i7-7700 4.0GHz).

The modeling effectiveness was scrutinized by comparing the calculated and measured settlements of the embankment for the real case (i.e. Sample 25 in Table 4). A displacement plate was installed on the ground surface at the center of cushion bottom (point B in Figure 3) to monitor the settlement of GRPSF over time. The time histories of the calculated and measured settlements and backfilling height are plotted in Figure 4. A good agreement between the two settlement histories was observed as shown in Figure 4. This comparison validated the adequacy of the GRPSF model in predicting the settlement.

For all other samples, the settlements of GRPSF at the base (i.e. point B as shown in Figure 3) during construction and services are presented in Figure 5. Intuitively, the post-construction settlement at the crest is more critical to the serviceability of the embankment, which is represented by the displacement at point A. The devolvement of the settlement at point A is depicted in Figure 6.

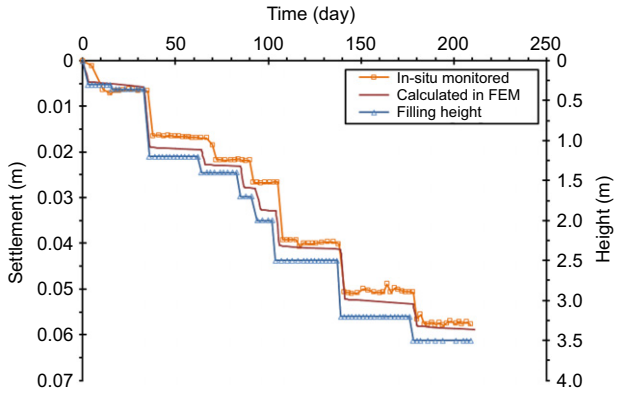

Figure 4. Calculated and measured settlement development of GRPSF during embankment filling

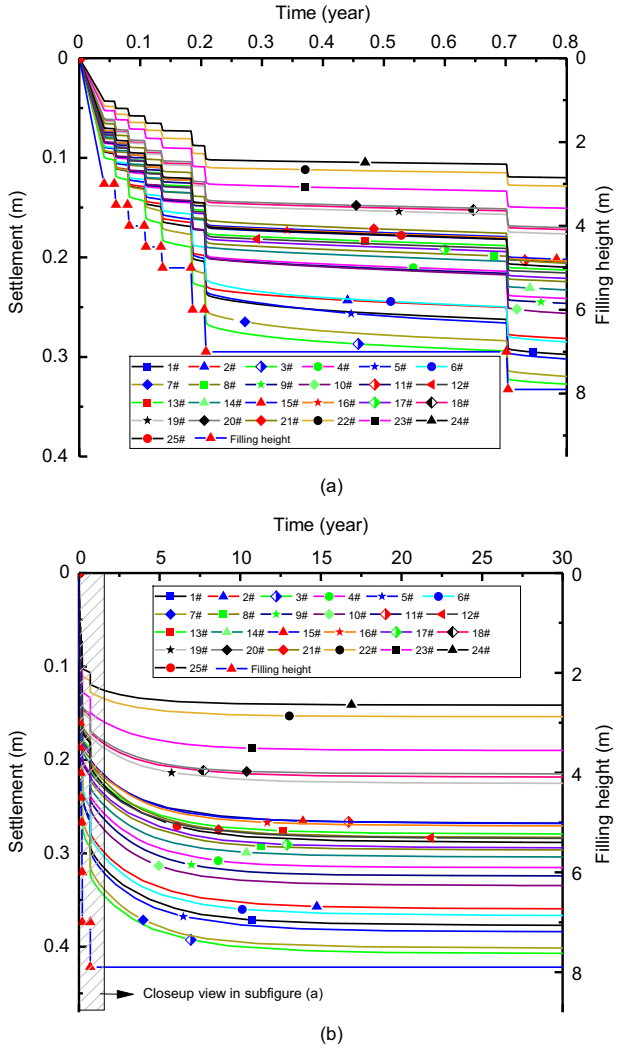

Figure 5. Settlement history of GRPSF samples: (a) construction stage; and (b) service stage

6.1.5. *Response of surrogate model*

Numerical modeling was used to calculate the post-construction settlement of GRPSF for each sample listed in Table 4. Settlements obtained from numerical modeling for the thirteen samples are presented in Table 5. Samples and their responses in Table 5, except for the 2nd, 9th, 12th, and 21st samples, were used to train the surrogate model based on the Kriging method. Thereafter, the surrogate model was applied to predict the responses for the 2nd, 9th, 12th, and 21st samples. The effectiveness of the surrogate model was validated by the comparison between the predicted and the numerical modeling responses. As shown in Table 5, the maximum deviation was 1.27%, which was found in the comparison of the

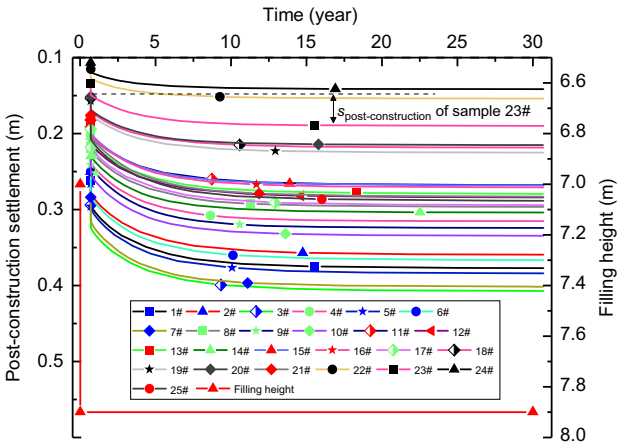

Figure 6. Time history of post-construction settlement of GRPSF samples

Table 5. Post-construction settlement response in numerical modeling

Sample	Calculated (m)	Predicted (m)	Relative error (%)	Type
1#	0.1147	0.1147	0.00	Trained
2#	0.1091	0.1095	−0.39	Tested
3#	0.1131	0.1131	0.00	Trained
4#	0.1013	0.1013	0.00	Trained
5#	0.1180	0.1180	0.00	Trained
6#	0.1168	0.1168	0.00	Trained
7#	0.1176	0.1176	0.00	Trained
8#	0.0976	0.0976	0.00	Trained
9#	0.1081	0.1082	−0.09	Tested
10#	0.1169	0.1169	0.00	Trained
11#	0.0859	0.0859	0.00	Trained
12#	0.0929	0.0927	0.24	Tested
13#	0.0910	0.0910	0.00	Trained
14#	0.1000	0.1000	0.00	Trained
15#	0.0890	0.0890	0.00	Trained
16#	0.0903	0.0903	0.00	Trained
17#	0.1000	0.1000	0.00	Trained
18#	0.0651	0.0651	0.00	Trained
19#	0.0683	0.0683	0.00	Trained
20#	0.0637	0.0637	0.00	Trained
21#	0.1072	0.1058	1.27	Tested
22#	0.0387	0.0387	0.00	Trained
23#	0.0562	0.0562	0.00	Trained
24#	0.0350	0.0350	0.00	Trained
25#	0.1068	0.1068	0.00	Trained

Table 6. Comparison between optimized and original design solutions for GRPSF

Design solution	l_p (m)	a (m)	s (m)	d (m)	h (m)	k (m)	Cost (USD/m)	$s_{post\text{-}construction}$ (m)	$s_{post\text{-}construction\text{-}FEM}$ (m)
Optimized	19.6	1.4	2.7	0.3	0.3	1	1706.9	0.0929	0.0943
Original	24	1.5	2.5	0.3	0.3	2	2805.4	0.1068	0.1068

21st sample. Such a difference in general is acceptable in engineering practice. It is noteworthy that all 25 samples were used as training samples when the surrogate model was applied to calculate the post-construction settlement in the following optimization process.

6.1.6. *Optimized design solution*

The construction cost of the GRPSF in case history A (i.e. Sample 25) was rewritten by

$$Q(x) = c_1 S_{\text{geogrid}} k + \left(c_2 V_{\text{pile-cap}} + c_3 V_{\text{pile}} + c_4 l\right)) \times n \tag{15}$$

in which c_1 denotes the price of geogrid per unit square meter; c_2 denotes the price of pile cap per unit cubic meter (assuming the same unit price for both cast-in-place and prefabricated pile caps); c_3 denotes the price of PHC pile per unit cubic meter (excluding the hollow space); c_4 denotes the price of pile connections per unit pile length (when the PHC pile is longer than 10 m, connections such as flange plates are needed); S_{geogrid} denotes the area of geogrid per layer; $V_{\text{pile-cap}}$ denotes the volume of each pile cap; V_{pile} denotes the volume of each pile (without the hollow volume); l_p denotes pile length; n denotes the number of piles. Specifically, the values for price parameters in Equation (16) were assigned according to the construction budget guidelines in China (MCHEQS 2018) as follows: $c_1 = 1.69$ USD/m^2; $c_2 = 57.52$ USD/m^3; $c_3 = 161.10$ USD/m^3; and $c_4 = 1.77$ USD/m.

According to the design code (MHURC 2012), the corrective factors β_p for pile and β_s for surrounding soil were set to 1.0 and 0.9, respectively. Then the optimization search in the sample space was performed using the aforementioned BH-GA algorithm, in which the response (post-construction settlement) for each sample was calculated using the Kriging surrogate model. The optimized design solution, – that is, the optimal values for design variables and the corresponding settlement response, as well as the original design solution is presented in Table 6. Because the allowable settlement is 100 mm (MT of China 2015), it is found that the optimized design solution succeeded in meeting the criteria (i.e. 92.9 mm) by using shorter pile length, smaller pile spacing, and single geogrid layer. In contrast, the original design solution failed to satisfy the settlement-based design demands even though it provided lower construction costs.

6.2. Case history B: soil-cement column-supported embankment

6.2.1. *Description*

Case history B was based on a trial embankment constructed in Saga, Japan (Igaya *et al.* 2011). The embankment had a height of 6.5 m and a crest width of 12 m. The subgrade was improved by 1.2 m diameter soil-cement columns that were installed in a square pattern with center-to-center spacing of 1.9 m. The schematic of this case history is shown in Figure 7, noting that no geosynthetic basal reinforcement was used (Chai *et al.* 2015). However, because the design variable k (the number of geogrid layers) could be assigned a value of zero, this case was considered as an effective GRPSF example in demonstrating the application of the presented optimization framework.

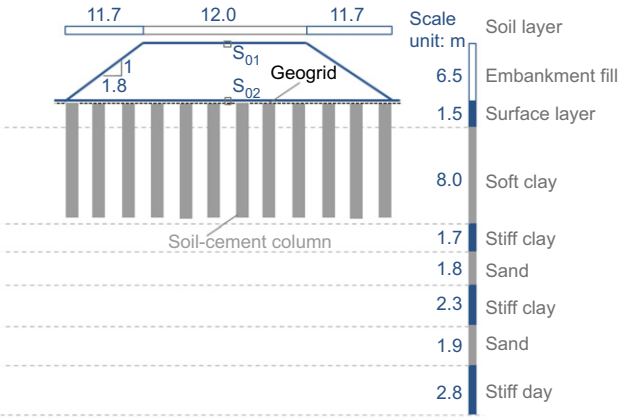

Figure 7. Schematic of case history B (redraw from Igaya *et al.* (2011))

Instrumentation was installed to monitor the deformation and pore water pressure. The acquired monitoring data at point S_{01} at the embankment crest was selected as the governing settlement indicator of GRPSF. Numerical modeling of this case history was carried out to calculate the deformation. It should be noted that the numerical model (ABAQUS) developed in this work was consistent with, but differed slightly in the mesh from, the 3D-2 model in Chai *et al.* (2015). Additionally, the post-construction settlement limit for this case was 0.3 m.

6.2.2. *Sampling using uniform design*

Because the soil-cement column-supported GRPSF in case history B did not use geogrid and pile cap, the design variables considered in the optimization analysis were pile diameter d, pile length l_p, and pile space s. The diameter of soil-cement column and the pile spacing are dependent on the construction technique, but their lower bounds are specified in design codes (MHURC 2012). The pile tip should be seated in the stiff clay layer. The variation and increment of the variables are presented in Table 7.

6.2.3. *Numerical and surrogate modeling*

Before analyzing the post-construction settlement at the crest of the embankment, the accuracy of FEM was

validated in this paper as shown in Figure 8. The case history (the original design solution) was numerically modeled using ABAQUS in a similar procedure used for case history A. The settlement of point S_{02} was monitored in numerical simulation and compared with in situ measured results (Chai *et al*. 2015) (as seen in Figure 8). The good agreement between the numerically calculated and in situ measured results validated the effectiveness and applicability of the numerical modeling in calculating the settlement of the designed embankment.

For all samples, the settlements of case B at the embankment base (i.e. point S_{01} as shown in Figure 7) during construction and services are presented in Figure 9. The Kriging method was also used to establish the surrogate model aiming at predicting the post-construction settlement based on training and tested samples as seen in Table 8. It is noted that the settlement histories of samples 1, 3, 4, and 7 were not available as FEM calculations were not convergent due to excessively

Table 7. Bounds and intervals for design variables of case history B

Design variable	d (m)	l_p (m)	s (m)
Lower and upper bounds	(0.5, 1.6)	(4, 10.9)	(1.5, 2.9)
Increment	0.1	0.3	0.2

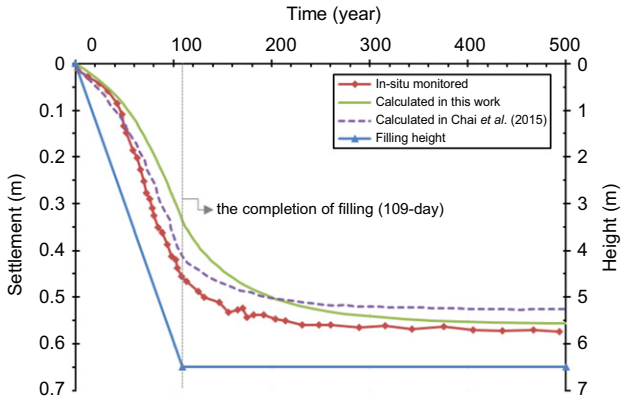

Figure 8. Time history of settlement at point S_{02} calculated using different methods

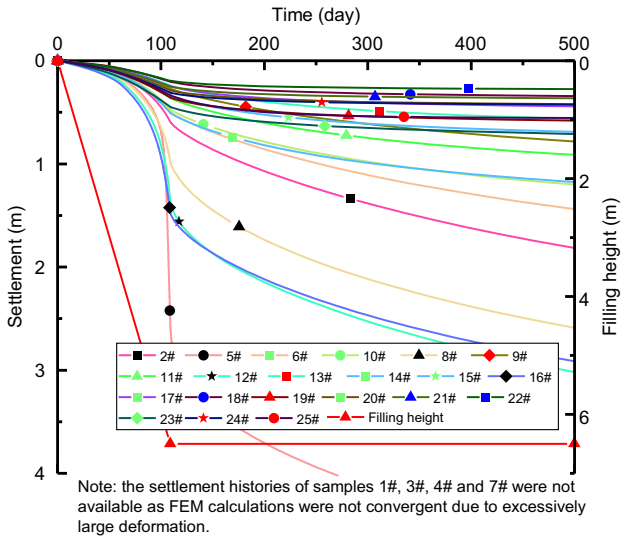

Figure 9. Time histories of settlement for samples of design solution

Table 8. Comparison of settlement between numerical and surrogate modelings

Sample	Calculated (m)	Predicted (m)	Relative error (%)	Type
1#	—	—	—	—
2#	1.2237	1.2237	0.00	Trained
3#	—	—	—	—
4#	—	—	—	—
5#	2.1355	2.1355	0.00	Trained
6#	0.9421	0.9421	0.00	Trained
7#	—	—	—	—
8#	1.6108	1.6108	0.00	Trained
9#	0.5119	0.5119	0.00	Trained
10#	0.7286	0.7286	0.00	Trained
11#	0.5504	0.5504	0.00	Trained
12#	1.6639	1.6639	0.00	Trained
13#	0.324	0.3240	0.00	Trained
14#	0.6699	0.6699	0.00	Trained
15#	0.3498	0.3496	0.07	Tested
16#	1.444	1.4440	0.00	Trained
17#	0.1951	0.1951	0.00	Trained
18#	0.1397	0.1397	0.00	Trained
19#	0.2226	0.2226	0.00	Trained
20#	0.1355	0.1355	0.00	Trained
21#	0.1138	0.1138	0.00	Trained
22#	0.0818	0.0818	0.00	Trained
23#	0.2633	0.2584	1.86	Tested
24#	0.1167	0.1167	0.00	Trained
25#	0.2194	0.2194	0.00	Trained

Table 9. Sampling of design variables using uniform design

Sample	l_p (m)	s (m)	d (m)
1#	4	1.7	1
2#	4.3	2.1	1.5
3#	4.6	2.5	0.8
4#	4.9	2.9	1.4
5#	5.2	1.7	0.7
6#	5.5	2.1	1.2
7#	5.8	2.5	0.5
8#	6.1	2.9	1.1
9#	6.4	1.7	1.6
10#	6.7	2.1	0.9
11#	7	2.5	1.5
12#	7.3	2.9	0.8
13#	7.6	1.5	1.3
14#	7.9	1.9	0.6
15#	8.2	2.3	1.2
16#	8.5	2.7	0.5
17#	8.8	1.5	1
18#	9.1	1.9	1.6
19#	9.4	2.3	0.9
20#	9.7	2.7	1.4
21#	10	1.5	0.7
22#	10.3	1.9	1.3
23#	10.6	2.3	0.6
24#	10.9	2.7	1.1
25#	8.5	1.9	1.2

Table 10. Optimized design parameters for case history B

Design solution	a (m)	l_p (m)	s (m)	Cost (USD/m)	$s_{post\text{-}construction}$ (m)	$s_{post\text{-}construction\text{-}FEM}$ (m)
Optimized	1.1	10	2.9	379.5	0.1289	0.1385
Original	1.2	8.5	1.9	793.4	0.2194	0.2194

large deformation. The predicted settlement results using the surrogate model were compared with the calculated settlement results in numerical modeling. Table 8 indicates that the maximum error is 1.864%, and higher prediction accuracy was found for the sample with a smaller settlement. The prediction capability of this settlement surrogate model was adequately verified.

Similar to the procedure used for case history A, evenly distributed samples were first generated for the surrogate model. The sample pool as seen in Table 9 includes 24 generated samples (the 1st–24th samples) and the as-built one (the 25th sample).

6.2.4. *Optimal results*

The construction cost of the stabilized foundation for case history B was calculated based on the optimized design solution obtained in the above-discussed procedure, as shown in Table 10. The corrective factors for pile β_p and surrounding soil β_s were set to 1.0 and 0.9, respectively. It is noted that the price of cement-soil column per unit length would increase, typically used in this calculation, by multiplying $1.05^{(d-0.5)/0.05}$ if the pile diameter d is greater than 0.5 m. It can be found that the construction cost of GRPSF was reduced to 379.5 USD per unit length of the embankment in the optimized design of this case. Specifically, the optimized design solution adopted the slightly reduced pile diameter and moderately increased pile length and pile spacing; and the post-construction settlement of the foundation was remarkably reduced to a quarter of the original design.

7. CONCLUSIONS

This work developed a novel optimization framework for Geogrid-Reinforced Pile-Supported Foundation (GRPSF) that is commonly used in ground improvement. An optimization model was established by defining the objective function in terms of construction cost and applying constraints on the basis of requirements on bearing capacity of soil and piles, shear and moment resistance of pile cap, and post-construction settlement of GRPSF. The Kriging method-based surrogate model was used in conjunction with FEM to calculate the GRPSF settlement. An integrated BH-GA algorithm was proposed to implement the global search of the optimized design solution with minimum construction cost. The major conclusions that can be drawn from this study are as follows:

(*a*) A cost optimization design framework of GRPSF was successfully developed, which could account for post-construction settlement, and various discrete design variables including pile length l_p, pile cap size a, pile spacing s, pile diameter d, pile cap thickness h, and the number of geogrid layers k.

(*b*) The integration of the Kriging method-based surrogate model and FEM computations was developed to implement an efficient and effective determination of post-construction settlement of GRPSF using a remarkably reduced number of design alternatives, – that is combinations of design variables.

(*c*) By introducing the selection and crossover operation of GA into the BH algorithm, the integrated BH-GA algorithm was applicable to a global search for optimization problems with both continuous and discrete variables, which can be used to solve many geotechnical problems in addition to the discussed GRPSF applications.

The presented framework is expected to provide a protocol of design optimization for GRPSF in design practice. It effectively balances the complexity and computational complexity and has a great potential for wide adoption in practice. Furthermore, this work is expected to provide insights into extensive applications of the hybrid of numerical simulation and surrogate modeling in optimizing construction costs for similar civil and infrastructure cases identified with discrete variables and implicit formulations of constraints.

ACKNOWLEDGMENTS

This research was sponsored by National Key Research Plan of China (2016YFC0800200), Natural Science Foundations of China (51978254, 51908201), and Natural Science Foundations of Hunan Province (2019JJ50150, 2020JJ5024). Their support is gratefully acknowledged.

APPENDIX

See Tables 11–14 and Figures 10 and 11.

Optimization formulations of two classical engineering problems are presented as follows:

Pressure vessel design problem.

Consider $\boldsymbol{x} = [x_1, x_2, x_3, x_4] = [T_s, T_h, R, L]$

$$\text{Minimize } F_8(\boldsymbol{x}) = 0.6224x_1x_3x_4 + 1.7781x_2x_3^2 + 3.1611x_1^2x_4 + 19.84x_1^2x_3 \quad (16)$$

Table 11. Information of benchmark functions used in the examination

Benchmark function	Range of variable	x_{gbest}	f_{min}	Type
$F_1(\boldsymbol{x}) = \sum_{i=1}^{D} x_i^2$	$(-100, 100)_D$	**0**	0	unimodal
$F_2(\boldsymbol{x}) = \sum_{i=1}^{D} \lvert -x_i + 5\rvert^2$	$(-100, 100)_D$	**5**	0	unimodal
$F_3(\boldsymbol{x}) = \sum_{i=1}^{D} \left(\sum_{j=1}^{i} x_j\right)^2$	$(-100, 100)_D$	**0**	0	unimodal
$F_4(\boldsymbol{x}) = \sum_{i=1}^{D} \lvert x_i\rvert + \prod_{i=1}^{D} \lvert x_i\rvert$	$(-10, 10)_D$	**0**	0	unimodal
$F_5(\boldsymbol{x}) = \sum_{i=1}^{D-1} \left(100\left(x_i^2 - x_{i+1}\right)^2 + \left(x_i - 1\right)^2\right)$	$(-100, 100)_D$	**0**	0	multimodal
$F_6(\boldsymbol{x}) = 20 + e - 20\exp\left(-0.2\sqrt{\frac{1}{D}\sum_{i=1}^{D} x_i^2}\right) - \exp\left(\frac{1}{D}\sum_{i=1}^{D}\cos(2\pi x_i)\right)$	$(-32, 32)_D$	**0**	0	multimodal
$F_7(\boldsymbol{x}) = 1/4000\sum_{i=1}^{D} x_i^2 - \prod_{i=1}^{D}\cos\left(x_i/\sqrt{i}\right) + 1$	$(-100, 100)_D$	**0**	0	multimodal

Notes: f_{min} and $\boldsymbol{x}_{gbest}$ are the minimum value and its position of the benchmark test function, respectively (bold values indicate all the elements in the variable vector are consistent with the same value); D denotes the dimension of the variable $\boldsymbol{x}$, which was set with the value of 10 for all benchmark functions.

Table 12. Minimum of benchmark functions solved using four optimization algorithms

Benchmark function	BH-GA		BH		GA		PSO	
	Continuous	Discrete	Continuous	Discrete	Continuous	Discrete	Continuous	Discrete
F_1	1.72×10^{-7}	0.00×10	1.88×10^{-10}	3.55×10	7.51×10^{-6}	1.00×10^{-2}	1.82×10^{2}	1.21×10
F_2	1.52×10^{-7}	0.00×10	8.24×10^{-10}	2.10×10^{-1}	2.52×10^{-6}	0.00×10	5.89×10^{2}	9.13×10^{1}
F_3	3.75×10^{-5}	6.00×10^{-2}	1.00×10^{-8}	4.36×10^{2}	1.24×10^{2}	3.23×10	3.19×10^{2}	2.52×10^{3}
F_4	1.26×10^{-3}	0.00×10	9.33×10^{-2}	4.90×10	9.54×10^{-5}	0.00×10	3.81×10	0.00×10
F_5	8.75×10^{-3}	5.12×10	9.27×10	5.48×10^{3}	1.78×10^{1}	6.48×10^{1}	1.38×10^{6}	2.40×10^{3}
F_6	6.70×10^{-4}	-8.88×10^{-16}	3.03×10	3.61×10	5.71×10^{-4}	-8.88×10^{-16}	7.93×10	3.61×10
F_7	7.55×10^{-4}	4.36×10^{-2}	2.01×10^{1}	7.77×10^{-1}	2.32×10	1.52×10^{-1}	1.64×10^{1}	0.00×10

Table 13. Optimal results for optimizing problem of pressure vessel

Algorithm	Optimal design variables				Minimum cost (US$)
	T_s	T_h	R	L	
BH-GA	0.8125	0.4375	42.0984	176.6369	6059.134
GA	1	0.5	51.6463	85.7981	6425.222
BH	0.8750	0.4375	45.3368	140.2540	6089.992
PSO	0.9375	0.75	46.2379	149.3638	8102.176
MVO (Seyedali *et al.* 2015)	0.8125	0.4375	42.0907	176.7387	6060.807

Table 14. Optimal results for optimizing problem of cantilever beam

Algorithm	Optimal design variables					Minimum weight (lb)
	x_1	x_2	x_3	x_4	x_5	
BH-GA	6.0101	5.3110	4.4977	3.5018	2.1531	1.339957
GA	5.8414	5.3418	4.6250	3.5118	2.1722	1.3411
BH	12.0180	8.2616	6.1819	5.3196	3.0749	2.1750
PSO	26.7417	26.6480	12.7289	9.8106	7.7842	5.2237
MVO (Seyedali *et al.* 2015)	6.0239	5.306	4.495	3.496	2.1527	1.349960

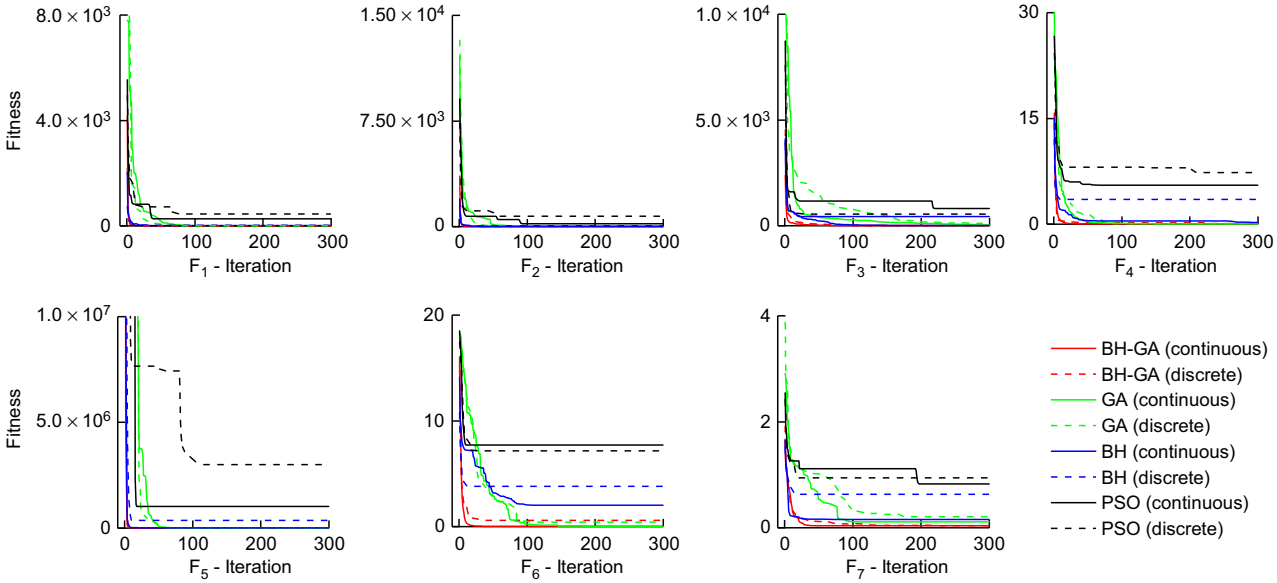

Figure 10. Fitness evolution of seven benchmark functions (F1–∼F7) over the iteration

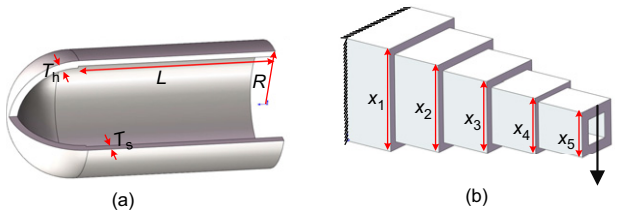

Figure 11. Schematics of classical engineering optimization problems: (a) pressure vessel; (b) cantilever beam

$$\text{Subject to}\begin{cases} -x_1 + 0.0193x_3 \le 0 \\ -x_2 + 0.00954x_3 \le 0 \\ -\pi x_3^2 x_4 - \frac{4}{3}\pi x_3^3 + 129600 \le 0 \\ 0.0625 \le x_1, x_2 \le 99 \times 0.0625 \\ 10 \le x_3 \le 200 \\ 10 \le x_4 \le 240 \end{cases}$$

Cantilever beam design problem.
Consider $\mathrm{x} = [x_1, x_2, x_3, x_4, x_5]$

$$\text{Minimize } F_9(\boldsymbol{x}) = 0.0624(x_1 + x_2 + x_3 + x_4 + x_5) \tag{17}$$

$$\text{Subject to}\begin{cases} \frac{61}{x_1^3} + \frac{27}{x_2^3} + \frac{19}{x_3^3} + \frac{7}{x_4^3} + \frac{1}{x_5^3} - 1 \le 0 \\ 0.01 \le x_1, x_2, x_3, x_4, x_5 \le 100 \end{cases}$$

NOTATION

Basic SI units are given in parentheses.

A_p cross-section area of a pile (m^2)
a pile cap size (m)
c_1 price of geogrid per unit square meter (USD/m^2)
c_2 price of pile cap per unit cubic meter (USD/m^3)
c_3 price of PHC pile per unit cubic meter (USD/m^3)
c_4 price of pile connections per unit pile length (USD/m)
d pile diameter (m)
$\boldsymbol{F}(\boldsymbol{x}, \beta)$ deterministic part of the regression model
f_{az} allowable bearing capacity (Pa)
f_{BH} fitness values of the black hole (dimensionless)
f_i fitness values of ith star (dimensionless)
f_{sk} capacity of surrounding soil (Pa)
f^T vector of regression functions
h pile cap thickness (m)
k number of geogrid layers (dimensionless)
L length of the cylinder except the head (in)
l_p pile length (m)
M moment force on pile cap (N·m)
M_R moment resistance of pile cap (N·m)
m area replacement ratio (dimensionless)
N number of stars (dimensionless)
n number of piles (USD/m^3)
p_{cz} soil overburden stress (Pa)
p_z additional stress induced by loading (Pa)
R inner radius (in)
R_a ultimate bearing capacity of the single pile (Pa)
R_{BH} event horizon of the black hole (dimensionless)
R_s axial load applied on the single pile (N)
$R(\boldsymbol{x}_i, \boldsymbol{x}_i^j)$ correlation function
r_1, r_2 learning factors (dimensionless)
$S_{geogrid}$ area of geogrid per layer (m^2)

s	pile spacing (m)
$s_{\text{post-construction}}$	post-construction settlement
T_{h}	thickness of the head (in)
T_{rupture}	rupture strength of geogrid
T_{s}	thickness of the shell (in)
V	shear force on pile cap (N)
V_{pile}	volume of each pile (without the hollow volume) (m^3)
$V_{\text{pile-cap}}$	volume of each pile cap (m^3)
V_{R}	shear resistance of pile cap (N)
$\boldsymbol{x}_{\text{BH}}$	position of the black hole in the search space (dimensionless)
$\boldsymbol{x}_{\text{best},t}$	the position of the best-fit individual in the tth iteration
$\boldsymbol{x}_i(t)$	positions of the ith star at the tth iteration (dimensionless)
y_i	response of the ith sampling point (dimensionless)
$Z(\text{x})$	stochastic process
β	regression coefficient
β_{p}	corrective factors for pile (dimensionless)
β_{s}	corrective factors for surrounding soil (dimensionless)
θ	parameters of correlation model
λ_i	the ith weight coefficient (dimensionless)

ABBREVIATIONS

BH	black hole
E	elastic
EP	elastic-perfect plastic
FEM	finite element method
GA	genetic algorithm
GRPSF	geogrid-reinforced pile-supported foundation
MOV	multi-verse optimizer
SLS	serviceability limit state
ULS	ultimate limit state

REFERENCES

Aldwaik, M. & Adeli, H. (2014). Advances in optimization of highrise building structures. *Structural and Multidisciplinary Optimization*, **50**, No. 6, 899–919.

Aldwaik, M. & Adeli, H. (2017). Cost optimization of reinforced concrete flat slabs of arbitrary configuration in irregular highrise building structures. *Structural and Multidisciplinary Optimization*, **54**, 151–164.

Ali, K., Shahu, J. T. & Sharma, K. G. (2014). Model tests on single and groups of stone columns with different geosynthetic reinforcement arrangement. *Geosynthetics International*, **21**, No. 2, 103–118.

Bagheri, S., Konen, W., Emmerich, M., Bäck, T. (2017). Self-adjusting parameter control for surrogate-assisted constrained optimization under limited budgets. *Applied Soft Computing*, **61**, 377–393.

Bouassida, M. & Carter, J. P. (2014). Optimization of design of column-reinforced foundations. *International Journal of Geomechanics*, **14**, No. 6, 04014031.

BSI (2010). *BS 8006: Code of Practice for Strengthened Reinforced Soil and Other Fills*, BSI, London, UK.

Chai, J. C., Shrestha, S., Hino, T., Ding, W. Q., Kamo, Y. & Carter, J. (2015). 2D and 3D analyses of an embankment on clay improved by soil–cement columns. *Computers and Geotechnics*, **68**, 28–37.

Chen, J. & Zhang, J. W. (2013). Calculation method for settlement of CFG pile-net composite foundation in high-speed railway. In *ICETCE '12 Proceedings of the 2012 Second International Conference on Electric Technology and Civil Engineering, Nanjing, China*, Peng, Q. & Wang, K., Editors, American Society of Civil Engineers (ASCE), Reston, VA, USA, pp. 2076–2081.

Chickermane, H. & Gea, H. (1996). Structural optimization using a new local approximation method. *International Journal for Numerical Methods in Engineering*, **39**, 829–846.

Chikahiro, Y., Ario, I., Pawlowski, P., Graczykowski, C. & Holnicki-Szulc, J. (2019). Optimization of reinforcement layout of scissor-type bridge using differential evolution algorithm. *Computer-Aided Civil and Infrastructure Engineering*, **34**, 523–538.

Gary, W. & Lucas, S. H. (1987). Design optimization of geosynthetic reinforced embankments over soft foundations. *Geotextiles and Geomembranes*, **6**, No. 1, 185–195.

Geddes, J. D. (1966). Stresses in foundation soils due to vertical subsurface loading. *Geotechnique*, **16**, No. 3, 231–255.

Ghalesari, A. T., Barari, A., Amini, P. F. & Ibsen, L. B. (2015). Development of optimum design from static response of pile–raft interaction. *Journal of Marine Science & Technology*, **20**, No. 2, 331–343.

Girout, R., Blanc, M., Thorel, L. & Dias, D. (2018). Geosynthetic reinforcement of pile-supported embankments. *Geosynthetics International*, **25**, No. 1, 37–49.

Goh, T. C., Zhang, Y. M., Zhang, R. H., Zhang, W. G. & Xiao, Y. (2017). Evaluating stability of underground entry-type excavations using multivariate adaptive regression splines and logistic regression. *Tunnelling and Underground Space Technology*, **70**, 148–154.

Han, J., Oztoprak, S., Parsons, R. L. & Huang, J. (2007). Numerical analysis of foundation columns to support widening of embankments. *Computers & Geotechnics*, **34**, No. 6, 435–448.

Hatamlou, A. (2013). Black hole: a new heuristic optimization approach for data clustering. *Information Sciences*, **222**, 175–184.

Hawchar, L., Soueidy, C. P. & Schoefs, F. (2018). Global kriging surrogate modeling for general time-variant reliability-based design optimization problems. *Structural and Multidisciplinary Optimization*, **58**, No. 3, 955–968.

Huang, J. & Han, J. (2010). Two-dimensional parametric study of geosynthetic-reinforced column-supported embankments by coupled hydraulic and mechanical modeling. *Computers & Geotechnics*, **37**, No. 5, 638–648.

Huang, J., Han, J. & Collin, J. G. (2005). Geogrid-reinforced pile-supported railway embankment- a three-dimensional numerical analysis. *Transport Research Board*, **1936**, No. 1, 221–229.

Igaya, Y., Hino, T. & Chai, J. C. (2011). Measured behavior of trial embankment on floating column improved soft Ariake clay deposit. *Lowland Technology International*, **13**, No. 1, 40–45.

Jamsawang, P., Yoobanpot, N., Thanasisathit, N., Voottipruex, P. & Jongpradist, P. (2016). Three-dimensional numerical analysis of a DCM column-supported highway embankment. *Computers & Geotechnics*, **72**, 42–56.

Jelušič, P. & Žlender, B. (2018). Optimal design of piled embankments with basal reinforcement. *Geosynthetics International*, **25**, No. 2, 150–163.

Jelušič, P. & Žlender, B. (2019). Determining optimal designs for geosynthetic-reinforced soil bridge abutments. *Soft Computing*, **24**, No. 5, 3601–3614.

Jelušič, P. & Žlender, B. (2020). Determining optimal designs for conventional and geothermal energy piles. *Renewable Energy*, **147**, 2633–2642.

Krige, D. G. (1953). A statistical approach to some basic mine valuation problems on the Witwatersrand. *Journal of the Chemical, Metallugical and Mining Engineering Society of South Africa*, **4**, No. 1, 18–18.

Leung, Y. F., Klar, A. & Soga, K. (2010). Theoretical study on pile length optimization of pile groups and piled rafts. *Journal of Geotechnical and Geoenvironmental Engineering*, **136**, No. 2, 319–330.

Li, L. H., Cui, F. L., Ferreira, P., Xiao, H. L. & Huang, J. (2019). Experimental study of embankments with different reinforcement

materials and spacing between layers. *Geotextiles and Geomembranes*, **47**, No. 4, 477–482.

Liang, F., Li, J. & Chen, L. (2006). Optimization of composite piled raft foundation with varied rigidity of cushion. In *Proceedings of GeoShanghai 2006*, Shanghai, China, Parsons, R. L., Zhang, L. M., Guo, W. D., Phoon, K. K. and Yang, M., Editors, American Society of Civil Engineers (ASCE), Reston, VA, USA, pp. 29–34,

Liu, K. W. & Rowe, R. K. (2015). Numerical modelling of prefabricated vertical drains and surcharge on reinforced floating column-supported embankment behaviour. *Geotextiles and Geomembranes*, **43**, No. 6, 493–505.

Lophaven, S. N., Nielsen, H. B. & Sondergaard, J. (2002). *DACE – A MATLAB Kriging Toolbox*. Technical report. IMM Technical University of Denmark, Lyngby, Denmark.

MCHEQS (Ministry of Communications Highway Engineering Quota Station) (2018). *JTGT-3832: Highway Engineering Budget Quota*, China Communication Press, Beijing, China.

MHURC (Ministry of Housing and Urban-Rural Construction of the People's Republic of China) (2012). *GB/T 50783: Technical Code for Composite Foundation*, China Planning Press, Beijing, China.

Michalewicz, Z. & Janikow, C. Z. (1991). Genetic algorithms for numerical optimization. *Statistics & Computing*, **1**, No. 2, 75–91.

Miro, S., Hartmann, D. & Schanz, T. (2014). Global sensitivity analysis for subsoil parameter estimation in mechanized tunneling. *Computers & Geotechnics*, **56**, 80–88.

MT of China (Ministry of Transport of the People's Republic of China) (2015). *JTGD30: Specification for Design of Highway Subgrades*, China Communication Press, Beijing, China.

Müthing, N., Zhao, C., Hölter, R. & Schanz, T. (2018). Settlement prediction for an embankment on soft clay. *Computers & Geotechnics*, **93**, 87–103.

Narsavage, P. A. (2019). Optimizing the design of driven pile foundations with instrumented static load tests. In *Proceedings of the Eighth International Conference on Case Histories in Geotechnical Engineering*, Philadelphia, PA, USA, Meehan, C. L., Kumar, S., Pando, M. A. and Coe, J. T., Editors, American Society of Civil Engineers (ASCE), Reston, VA, USA, pp. 93–106.

Ng, K. S. & Tan, S. A. (2015). Settlement prediction of stone column group. *International Journal of Geosynthetics and Ground Engineering*, **1**, No. 4, 1–13.

Phutthananon, C., Jongpradist, P., Jongpradist, P., Dias, D. & Baroth, J. (2020). Parametric analysis and optimization of T-shaped and conventional deep cement mixing column-supported embankments. *Computers and Geotechnics*, **122**, 103555.

Piotrowski, A. P., Napiorkowski, J. J. & Rowinski, P. M. (2014). How novel is the "novel" black hole optimization approach? *Information Sciences*, **267**, 191–200.

Sacks, J., Welch, W. J., Mitchell, T. J. & Wynn, H. P. (1989). Design and analysis of computer experiments. *Statistical Science*, **4**, No. 4, 409–435.

Sandgren, E. (1990). Nonlinear integer and discrete programming in mechanical design optimization. *Journal of Mechanical Design*, **122**, No. 2, 223–229.

Schoefs, S. F., Le, K. T. & Lanata, F. (2013). Surface response meta-models for the assessment of embankment frictional angle stochastic properties from monitoring data: an application to harbour structures. *Computers and Geotechnics*, **53**, 122–132.

Seyedali, M., Abdolreza, H. & Seyed, M. M. (2015). Multi-verse optimizer: a nature-inspired algorithm for global optimization. *Neural Computing and Applications*, **27**, No. 2, 495–513.

Shen, P., Xu, C. & Han, J. (2020). Centrifuge tests to investigate global performance of geosynthetic-reinforced pile-supported embankments with side slopes. *Geotextiles and Geomembranes*, **48**, No. 1, 120–127.

Slem, M. B. & Tomaso, L. (2018). Automatic selection for general surrogate models. *Structural and Multidisciplinary Optimization*, **58**, 719–734.

Song, T., Pu, H., Schonfeld, P., Zhang, H., Li, W., Hu, J. P. & Wang, J. (2020). Mountain railway alignment optimization considering geological impacts: a cost-hazard bi-objective model. *Computer-Aided Civil and Infrastructure Engineering*, **35**, 1–22.

Suganthan, P. N., Hansen, N., Liang, J. J., Deb, K., Chen, Y. P., Auger, A. & Tiwari, S. (2005). *Problem Definitions and Evaluation Criteria for the CEC 2005 Special Session on Real-Parameter Optimization*. Technical Report, Nanyang Technological University, Singapore & Kanpur Genetic Algorithms Laboratory, Kanpur, India.

Suro, S. M., Bakar, I. & Sulaeman, A. (2016). Pile spacing optimization of short piled raft foundation system for obtaining minimum settlement on peat. *IOP Conference Series: Materials Science and Engineering*, Bakar, I. H., Editor, Institute of Physics (IOP), Langkawi, Malaysia, vol. 136, pp. 1–7.

TPDI (Guangdong Transportation Planning and Design Institute Limited) (2016). *Engineering Geological Investigation Report of the First Phase of Shanwei Section of Xingning-Shanwei Expressway*, TPDI, Guangzhou, China.

Wang, Y. (2009). Reliability-based economic design optimization of spread foundation. *Journal of Geotechnical and Geoenvironmental Engineering*, **135**, No. 7, 954–959.

Wang, B. L., Zhou, S. H. & Wang, C. D. (2011). Settlement calculation method with pile-net composite foundation. In *Proceedings of the 11th International Conference of Chinese Transportation Professionals (ICCTP), Nanjing, China*. Yin, Y. F., Wang, Y. H., Lu, J. and Wang, W., Editors, American Society of Civil Engineers, Reston, VA, USA.

Wijerathna, M. & Liyanapathirana, D. S. (2019). Load transfer mechanism in geosynthetic reinforced column- supported embankments. *Geosynthetics International*, **27**, No. 3, 236–248.

Wu, J. T., Ye, X., Li, J. & Li, G. W. (2019). Field and numerical studies on the performance of high embankment built on soft soil reinforced with PHC piles. *Computers and Geotechnics*, **107**, 1–13.

Zhang, J., Liu, K., Tan, Y. & He, X. (2008). Random black hole particle swarm optimization and its application. In *Proceedings of the 2008 International Conference on Neural Networks & Signal Processing, Nanjing, China*. Institute of Electrical and Electronics Engineers (IEEE), Piscataway, NJ, USA, pp. 359–365.

Zhang, W. G., Zhang, Y. M. & Goh, T. C. (2017). Multivariate adaptive regression splines for inverse analysis of soil and wall properties in braced excavation. *Tunnelling and Underground Space Technology*, **64**, 24–33.

Zhang, W. G., Zhang, R. H., Wang, W., Zhang, F. & Goh, A. (2019). A multivariate adaptive regression splines model for determining horizontal wall deflection envelope for braced excavations in clays. *Tunnelling and Underground Space Technology*, **84**, 461–471.

Zhao, C., Hölter, R., König, M. & Lavasan, A. A. (2019). A hybrid model for estimation of ground movements due to mechanized tunnel excavation. *Computer-Aided Civil and Infrastructure Engineering*, **34**, 586–601.

Zheng, J. J., Abusharar, S. W. & Wang, X. Z. (2008). Three-dimensional nonlinear finite element modeling of composite foundation formed by CFG–lime piles. *Computers & Geotechnics*, **35**, No. 4, 637–643.

Zheng, G., Yu, X., Zhou, H., Wang, S., Zhao, J., He, X. & Yang, X. (2020). Stability analysis of stone column-supported and geosynthetic-reinforced embankments on soft ground. *Geotextiles and Geomembranes*, **48**, No. 3, 349–356.

Zhou, M., Liu, H. L., Chen, Y. M. & Hu, Y. X. (2016). First application of cast-in-place concrete large-diameter pipe (PCC) pile-reinforced railway foundation: a field study. *Canadian Geotechnical Journal*, **53**, No. 4, 708–716.

The Editor welcomes discussion on all papers published in Geosynthetics International. Please email your contribution to discussion@geosynthetics-international.com by 15 April 2022.